INSTITUTE OF PHYSICS PUBLISHING PHYSICS IN MEDICINE AND BIOLOGY

Phys. Med. Biol. **49** (2004) 3291–3305 PII: S0031-9155(04)77091-8

K-edge digital subtraction imaging based on a dichromatic and compact x-ray source

A Sarnelli[1], A Taibi[1], A Tuffanelli[1], G Baldazzi[2], D Bollini[2], A E Cabal Rodriguez[3], M Gombia[2], F Prino[4], L Ramello[4], E Tomassi[4] and M Gambaccini[1]

[1] Dipartimento di Fisica dell'Università di Ferrara and INFN Sezione di Ferrara, Via Paradiso 12, I-44100 Ferrara, Italy
[2] Dipartimento di Fisica dell'Università di Bologna and INFN Sezione di Bologna, Viale Berti Pichat 64/2, 40127 Bologna, Italy
[3] CAEDAN, Havana, Cuba
[4] Dipartimento di Scienze e Tecnologie Avanzate, Università del Piemonte Orientale and INFN Sezione di Alessandria, C.so, Borsalino 54, I-15100 Alessandria, Italy

E-mail: sarnelli@fe.infn.it

Received 3 March 2004
Published 5 July 2004
Online at stacks.iop.org/PMB/49/3291
doi:10.1088/0031-9155/49/14/019

Abstract

This work proposes a compact dichromatic imaging system for the application of the K-edge digital subtraction technique based on a conventional x-ray tube and a monochromator system. A quasi-monochromatic x-ray beam at the energy of iodine K-edge is produced by Bragg diffraction on a mosaic crystal. Two thin adjacent beams with energies that bracket the K-edge discontinuity are obtained from the diffracted beam by means of a proper collimation system. They are then detected using an array of Si detectors. A home-made phantom is used to study the image quality as a function of iodine concentration. Signal and signal-to-noise ratio analysis has also been performed. The results are compared with theoretical expectations.

1. Introduction

In contrast-enhanced dual-energy subtraction imaging two images, acquired at different energies after the contrast media administration, are subtracted to highlight structures uptaking contrast media. K-edge digital subtraction (KES) imaging takes advantage of the sharp rise of the absorption coefficient of a suitable contrast agent performing the simultaneous acquisition of two images after the injection of the contrast agent at energies just below and above the K-edge energy. The logarithmic subtraction of the low- and high-energy

 © 2004 IOP Publishing Ltd Printed in the UK

images results in a final image with excellent sensitivity to the structures perfused by contrast agent and minimal sensitivity to the other ones. The main application of the KES technique is the coronary angiography that uses an iodinated contrast agent. The enhancement in sensitivity allows the intravenous injection of the contrast agent and this leads to a remarkable risk reduction with respect to conventional angiography. The K-edge digital subtraction angiography has been fully tested by using synchrotron radiation and several research protocols have been designed to evaluate the performance of this method in comparison with the conventional one. At the European Synchrotron Radiation Facility (ESRF) a medical beamline has been dedicated for medical applications of synchrotron radiation (Elleaume *et al* 1999, Dabin *et al* 2001). The results obtained with the first patients at the ESRF medical beamline are reported by Elleaume *et al* (2000). Several patients were imaged and excellent image quality was obtained together with a good agreement in terms of stenosis diagnosis between synchrotron angiography and the usual angiography procedure in hospital. The latest and largest study with a fixed protocol and an unchanged system was carried out at the HASYLAB at DESY in Hamburg, Germany (Dix *et al* 2003). Two hundred and thirty patients were investigated with the NIKOS IV system (Dix 1995, Dill *et al* 1998) and the study demonstrated the feasibility and safety of the method and its ability to provide useful information and diagnostic accuracy. Most problems with unevaluable segments depend on the projection angle and the superposition on the left ventricle, the aorta or pulmonary veins. Others problems arise from a low signal-to-noise ratio in overweight patients.

Preliminary studies have demonstrated that dual-energy contrast-enhanced mammography is also a promising technique for the detection of breast cancers. Skarpathiotakis *et al* (2002) reported a preliminary consideration about the physics and technical issues involved in contrast digital mammography. The method is based on the acquisition of an initial 'mask' image followed by one or more images obtained after contrast agent has been administered. Then the logarithm of the mask image is subtracted from the logarithm of each post contrast image. A molybdenum anode x-ray tube with a copper filtration allows one to effectively shape the x-ray spectrum to maximize the proportion of x-ray with energies above the K-edge of iodine. Simple logarithmic subtraction is found to be adequate in suppressing background signals. The technique proposed by Lewin *et al* (2003) consists of high- and low-energy digital mammography after the administration of iodinated contrast agent. Weighted subtraction of the logarithmic images allows one to remove the background morphology and to highlight structures hidden in the absence of contrast media. To maximize the sensitivity of this imaging technique when using the low concentrations of contrast agent, the x-ray spectrum should be shaped so that the x-rays have energies that are just above the K-edge of the contrast medium.

The development of compact sources has been discussed in the paper of Zhong *et al* (1997) and in references therein. A low intensity prototype, based on rotating anode source and a bent Laue monochromator, was evaluated for dual-energy digital subtraction angiography. The authors concluded that a useful photon flux could be achieved with an optimization of the optical system. We have been investigating for many years the production and possible clinical use of quasi-monochromatic x-ray sources by using Bragg diffraction on mosaic crystals. Prototype imaging systems were studied both for mammography (Gambaccini *et al* 1996, 1999) and computed tomography applications (Del Guerra *et al* 2003). This paper reports the development and test of a compact dichromatic imaging system for the application of the K-edge digital subtraction technique. Iodine phantom imaging was performed as a function of concentration to assess the image quality of the proposed system. A comparison with the theoretical model is also presented.

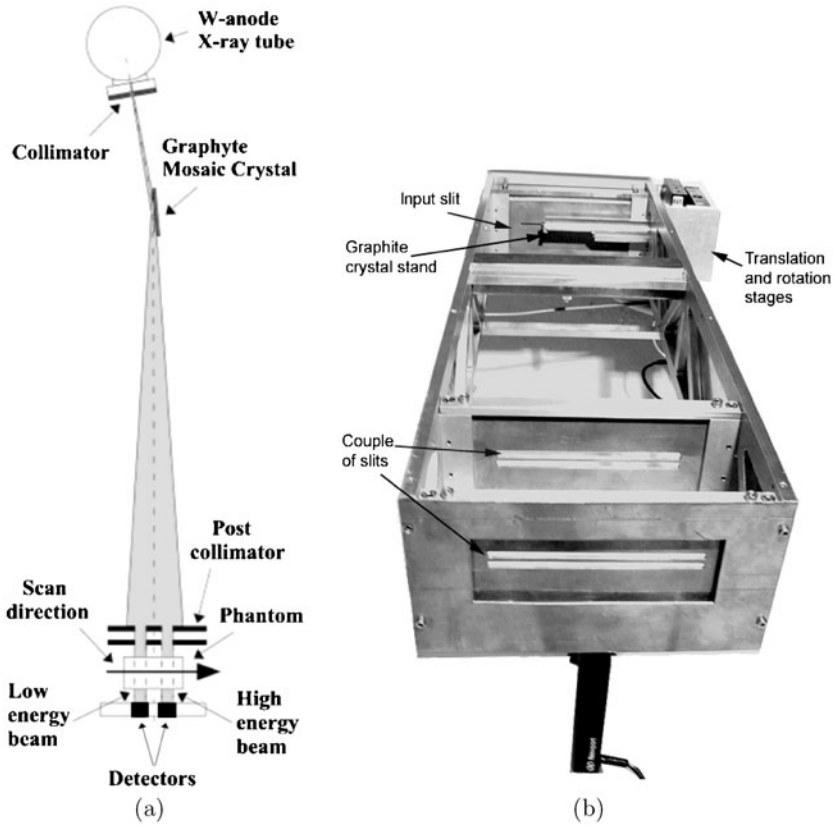

Figure 1. (a) Layout of the dichromatic imaging system (side view). (b) A photograph of the optical system (top view).

2. Materials and methods

2.1. Description of the source

Quasi-monochromatic x-ray beams are produced via Bragg diffraction on highly oriented pyrolytic graphite mosaic crystals (Gambaccini *et al* 1995). It has been demonstrated that mosaic crystals produce a wider energy bandpass compared to perfect crystal and provide an excellent choice as monochromator for applications requiring high photon fluxes as medical imaging (Tuffanelli *et al* 1999). Furthermore, spatial resolution measurements showed that the focal spot size depends on mosaic characteristics and geometrical set-up (Gambaccini *et al* 1995).

The imaging system is schematically depicted in figure 1. The photon source consists of a conventional W-anode Al-filter x-ray tube, operating at 65 kVp. The applied tube potential was chosen both to optimize photon flux and to avoid photons of second diffraction order. Polychromatic x-rays emerging from the tube window are collimated and impinge on the crystal with an incidence angle of 3.2°, which is the Bragg angle at the iodine K-edge energy (33.17 keV). The positioning of the mosaic crystal is performed by means of precision translation and rotation servo controlled stages. The crystal is supplied by Optigraph (Moscow, Russia); the size is $28 \times 60 \times 1$ mm^3 and the measured mosaic spread is 0.26°. The diffracted

Table 1. Main characteristics of the quasi-monochromatic beams. The energy resolution is calculated in terms of FWHM.

	Mean energy (keV)	Intensity ph $(mAs)^{-1}$ mm^{-2}	Energy resolution (keV)	(%)
Peak I	31.2	2.4×10^4	2.5	7.9
Peak II	35.6	1.0×10^4	3.0	8.3

quasi-monochromatic beam is split into two separated beams by means of two micrometrically adjustable double collimation systems placed in front of the radiographic plane. The distance between the two double collimators is 100 mm. Each collimator system has two slits 120 mm long, 4.0 mm wide separated by 6 mm. The x-ray tube focus-to-crystal and crystal-to-output collimator distances are set to 130 mm and 570 mm, respectively.

A computer simulation was previously performed to design the optical system with the available crystal and to optimize the characteristics of the dual-energy source in terms of energy resolution, photon flux, size and separation of the diffracted beams (Tuffanelli *et al* 2002a, 2002b). Results showed that the energy profiles of the two diffracted beams do not overlap and the mean energy lower and higher than the iodine K-edge is 31.2 keV and 35.6 keV, respectively. Since the mosaic crystal thickness used with this prototype x-ray source is not optimized for the iodine K-edge energy, the ratio between measured photon fluxes at low and high energy is 2.4 (Baldazzi *et al* 2002). Furthermore, the x-ray spectrum of the polychromatic beam is not flat in the energy range of interest, thus affecting the intensity of the two diffracted beams. Table 1 summarizes the measured spectral characteristics of the two x-ray beams.

2.2. Phantom

The test object used is the step wedge phantom shown in figure 2. It consists of four Plexiglas bulks 10 mm thick and 30 mm wide, with length ranging from 15 to 45 mm. The bulk at the bottom contains four cylindrical cavities with the same diameter and each cavity is placed in correspondence with a step. By means of lateral catheters the cavities are filled with a suitable concentration of the contrast medium. An aluminium layer, 2 mm thick, is placed in contact with the three Plexiglas bulks. These superimposed aluminium and Plexiglas layers simulate the bone and soft tissue so as to disturb vessel visualization. The detailed structure of the phantom is the following: step 1 is a bulk of 40 mm of Plexiglas and 6 mm of aluminium; step 2 is a bulk of 30 mm of Plexiglas and 4 mm of aluminium; step 3 is a bulk of 20 mm of Plexiglas and 2 mm of aluminium; step 4 is a bulk of 10 mm of Plexiglas. Two similar phantoms, with a vessel diameter of 1 mm and 2 mm were used in the experiment.

2.3. Detection system

Images of the phantom have been acquired at the two energies of the dichromatic beam using a detection system capable of single photon counting. The detector is a prototype (Baldazzi *et al* 2003a, 2003b, 2003c) based on an array of 384 silicon microstrips equipped with read-out electronics of 6 RX64 ASICs: each strip is 1 cm long, has a pixel pitch of 100 μm and a depth of 300 μm. We used the detection system in edge-on configuration, i.e putting the microstrips parallel to the incoming beam. The total detection surface is 38.4×0.3 mm^2. The single RX64 ASIC integrates 64 channels of front-end (preamplifier, shaper, discriminator) and

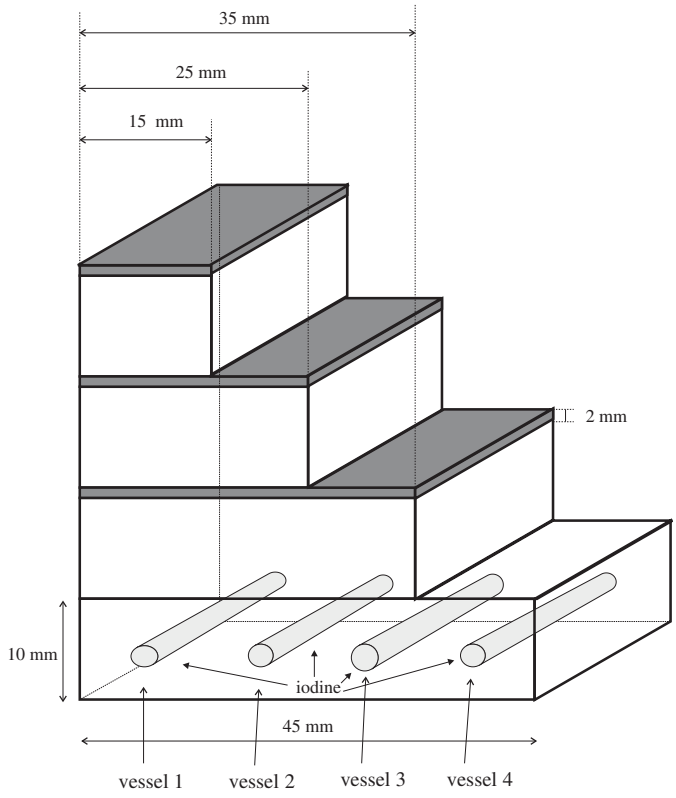

Figure 2. Schematic of the test object structure.

64 counters with 20 bit range. In this way it can simultaneously process signals and store data from 64 microstrips. The main features of RX64 ASIC are low noise (operation with threshold as low as 6 keV is possible) and good counting rate capability of 100–200 kHz per channel. More details on the ASIC design and performance are given by Grybos and Dabrowski (2001).

The edge-on configuration assures a good spatial resolution ($100 \times 300\ \mu m^2$) and a very good efficiency in the energy range of interest because the detection active length is 10 mm. The detector efficiency, calculated by taking into account the attenuation produced by the inactive Si layer of 0.750 mm and the absorption of 10 mm length strip, is 76% at 31.2 keV and 75% at 35.6 keV.

Before the acquisition of the phantom images, we tested the response of the detector by using quasi-monochromatic x-rays with high rate. We observed that the six chips have different efficiency when high photon flux impinges on the detector surface, probably due to the very high counting rate. This inefficiency affects the image quality because it introduces a systematic error which will be discussed in section 4.

2.4. Image acquisition

Two images at 31.2 keV and 35.6 keV have been recorded with iodine concentrations ranging from 370 mg ml^{-1} to 11.6 mg ml^{-1}. The substance used is Ultravist® (iopromide, 370 mg ml^{-1} iodine, density 1.4 g ml^{-1}). The images were recorded by performing a scan of

the phantom along the direction orthogonal to the diffracted beam. The exposure condition for a single scan was: 65 kV, 40 mA; the acquisition time was 1 s. Images are composed from 20 scans, resulting in a matrix of 20 × 384 pixels. The images are weighed by means of the correspondent flat field, i.e the images of the field produced by the source at two different energies acquired without the test object. This procedure allows us to take into account the incident beam non-uniformities and to correct the pattern noise due to individual efficiencies of detector elements.

3. Image processing

In conventional K-edge digital subtraction two monochromatic x-ray beams, whose energies are just below and above the iodine K absorption edge, are used. In the raw images the signal is proportional to the number of photons impinging on the detector after the transmission through the object:

$$N(E_{\pm}) = N_0(E_{\pm}) \exp\left\{ -\sum_i \left[\frac{\mu}{\rho}(E_{\pm}) \right]_i (\rho t)_i \right\} \tag{1}$$

where N_0 is the mean number of incident photons per area unit, E_+ and E_- are the two energies that bracket the K-edge discontinuity, μ/ρ is the mass attenuation coefficient, ρ is the density of materials, t is the transmitted path length. The subscript i denotes the different materials that compose the phantom (iodine solution, Plexiglas and aluminium).

The digital subtraction is based on the logarithmic subtraction of the two images. Since the energy separation of the two quasi-monochromatic x-ray beams is about 4 keV, the variation of the absorption coefficients for the background structures is not negligible in the logarithmic subtraction. This means that, besides the iodine signal, in the subtracted image there is a spurious background arising from an incomplete cancellation of contrast arising from other materials. However, it is possible to calculate an *iodine* image from the two energy images. In fact, it has been shown (Lehmann *et al* 1981) that the dual energy method allows decomposing the sample in only two basis materials. This method considers the linear attenuation coefficient of two basis materials to form an orthogonal coordinate system where each point represents a certain mixture of the two basis materials. We chose as basis materials *iodine* and *water* and in this way the element *iodine* can be distinguished from the fictitious 'element' *water* which comprises all other materials. If the beams are assumed to be monochromatic, equation (1) can be rewritten as a function of the two basis materials:

$$\ln \frac{N}{N_0}(E_{\pm}) = \left[\frac{\mu}{\rho}(E_{\pm}) \right]_{\text{iodine}} \cdot (\rho t)_{\text{iodine}} + \left[\frac{\mu}{\rho}(E_{\pm}) \right]_{\text{water}} \cdot (\rho t)_{\text{water}} \tag{2}$$

where $(\mu/\rho)_{\text{iodine}}$ and $(\mu/\rho)_{\text{water}}$ are the mass absorption coefficient of the iodine and water at energies of interest, $(\rho t)_{\text{iodine}}$ is the mass density of iodine, while $(\rho t)_{\text{water}}$ is the water equivalent mass density of all other materials. The quantities μ/ρ at the two energies E_+ and E_- are known, while the mass densities ρt of iodine and water are unknown quantities independent of the energies. These latter quantities can be calculated, pixel by pixel, by solving the two logarithmic transmissions in equation (2). In this way two final images are obtained from the raw images: the *iodine* image and the *water* image. They are given by

$$(\rho t)_{\text{iodine}} = \frac{\left[\frac{\mu}{\rho}(E_-)\right]_{\text{water}} \cdot \ln \frac{N_0}{N}(E_+) - \left[\frac{\mu}{\rho}(E_+)\right]_{\text{water}} \cdot \ln \frac{N_0}{N}(E_-)}{K_0} \tag{3}$$

$$(\rho t)_{\text{water}} = \frac{\left[\frac{\mu}{\rho}(E_+)\right]_{\text{iodine}} \cdot \ln \frac{N_0}{N}(E_-) - \left[\frac{\mu}{\rho}(E_-)\right]_{\text{iodine}} \cdot \ln \frac{N_0}{N}(E_+)}{K_0} \tag{4}$$

where

$$K_0 = \left[\frac{\mu}{\rho}(E_-)\right]_{\text{water}} \cdot \left[\frac{\mu}{\rho}(E_+)\right]_{\text{iodine}} - \left[\frac{\mu}{\rho}(E_+)\right]_{\text{water}} \cdot \left[\frac{\mu}{\rho}(E_-)\right]_{\text{iodine}}. \tag{5}$$

The *iodine* image is the map of contrast medium concentration while the *water* image includes all other materials.

3.1. Evaluation of signal and SNR

To evaluate the image quality the signal and the signal-to-noise ratio (SNR) have been measured on the *iodine* images.

The signal S produced by the vessel filled with iodine is measured on the transversal profile of the vessel as the difference between the peak value and the background value. The peak value is the average number of counts calculated on 20 pixels in correspondence with the diameter of the vessel; the background value is the average signal produced in a region surrounding the vessel.

The SNR is the ratio between the signal produced by the detail of interest and the background noise, σ_{bg}:

$$\text{SNR} = \frac{S}{\sigma_{\text{bg}}}. \tag{6}$$

To measure the σ_{bg} we sampled the image background in several areas. The area of the object to be detected is taken as the sampling area (Wagner 1977). The sampling area for background noise is 3 mm^2. The size of area has been chosen to maximize the sampling and to obtain good statistics. The standard deviation of the mean number of counts inside these areas is σ_{bg}.

3.2. Theoretical analysis of signal and SNR

In order to understand the expected signal and SNR in the *iodine* image, a theoretical evaluation has been performed. The signal of the vessel is given by the difference between the value of $(\rho t)_{\text{iodine}}$ in correspondence with the full diameter with the vessel (peak value) and the background. In our phantom the actual transmission in correspondence with the vessel is given by

$$\ln \frac{N_0}{N_v} = \mu_c t_c + \mu_p (t_p - t_c) \tag{7}$$

while for the background it is given by

$$\ln \frac{N_0}{N_b} = \mu_p t_p \tag{8}$$

where N_v and N_b indicate the mean number of detected photons per area unit in correspondence with the vessel and the background respectively, μ_c and μ_p are the linear absorption coefficients of the contrast medium and Plexiglas, respectively; t_c is the vessel diameter and t_p is the Plexiglas thickness containing the vessel. The signal S in the *iodine* image can be calculated substituting equations (7) and (8) in equation (3), therefore:

$$S = \frac{\left[\frac{\mu}{\rho}(E_-)\right]_{\text{water}} \cdot \mu_c(E_+) - \left[\frac{\mu}{\rho}(E_+)\right]_{\text{water}} \cdot \mu_c(E_-)}{K_0} \cdot t_c - \frac{\left[\frac{\mu}{\rho}(E_-)\right]_{\text{water}} \cdot \mu_p(E_+) - \left[\frac{\mu}{\rho}(E_+)\right]_{\text{water}} \cdot \mu_p(E_-)}{K_0} \cdot t_c. \quad (9)$$

The contrast medium is composed of iopromide salt, that contains iodine, in aqueous solution. For the sake of simplicity, it is possible to treat the contrast medium as a solution of iodine and water. The mass attenuation coefficient, $(\mu/\rho)_c$ has been calculated using the following equation:

$$(\mu/\rho)_c = w_{\text{water}}(\mu/\rho)_{\text{water}} + w_{\text{iodine}}(\mu/\rho)_{\text{iodine}} \quad (10)$$

where w_{water} and w_{iodine} are the fraction by weight of water and iodine, respectively; the fraction by weight of other elements composing the iopromide salt has been neglected.

Assuming that the signal fluctuations are dominated by Poisson statistics and the other contributions can be neglected, the noise for the area unit can be expressed as

$$\sigma^2_{\text{Poisson}} = \left[\frac{\left[\frac{\mu}{\rho}(E_-)\right]_{\text{water}}}{K_0}\right]^2 \cdot \frac{1}{N(E_+)} + \left[\frac{\left[\frac{\mu}{\rho}(E_+)\right]_{\text{water}}}{K_0}\right]^2 \cdot \frac{1}{N(E_-)}. \quad (11)$$

The background noise in the area of interest is the standard deviation of the mean of counts and can be obtained as

$$\sigma_{\text{bg}} = \frac{\sigma_{\text{Poisson}}}{\sqrt{A}} \quad (12)$$

where σ_{Poisson} is calculated for unit area and A is the value of the area of interest in area unit. The quantum limited curve of SNR was obtained by dividing equation (9) by equation (12).

4. Results and discussion

For each concentration the *iodine* and *water* images have been obtained. The mean incident photon fluence for each scan was 9.6×10^5 photons mm^{-2} for low energy and 4.0×10^5 photons mm^{-2} for high energy. The surface dose to the phantom was 5.3×10^{-2} mGy for the low energy and 1.7×10^{-2} mGy for the high energy.

In figure 3 the two energy images and the *iodine* and *water* images with the respective profiles are shown for the test object with vessel diameter equal to 2 mm and an iodine concentration of 370 mg ml^{-1}. In the *iodine* image the background structures are not visible and the iodine signal is isolated. In the *water* image only the step wedge phantom structure is evident. The profiles are the average of counts calculated for the 20 scans. Figures 4 and 5 show the *iodine* images and the profiles for the two phantoms as a function of iodine concentration.

Figures 4 and 5 show that the signal decreases with the concentration for a fixed diameter. By comparing two images with the same concentration (see figure 6), it is possible to appreciate the vessel signal variation with different diameters. For the lowest concentrations (see figures 4(f) and 5(e), (f)) the signals become comparable with the noise fluctuations for some vessels and it is not possible to distinguish them. The signal produced by the second cavity (see figure 2) appears lower than the others and the corresponding background shows discontinuities. This is evident in particular in figures 4(d) and 5(b). As mentioned in section 2.3, this effect is due to the response of detector read-out chips. The mismatch between the efficiencies of chips introduced a systematic error that lowered the SNR. In particular, the counter of the second read-out chip, that corresponds to pixels 128–192, showed different

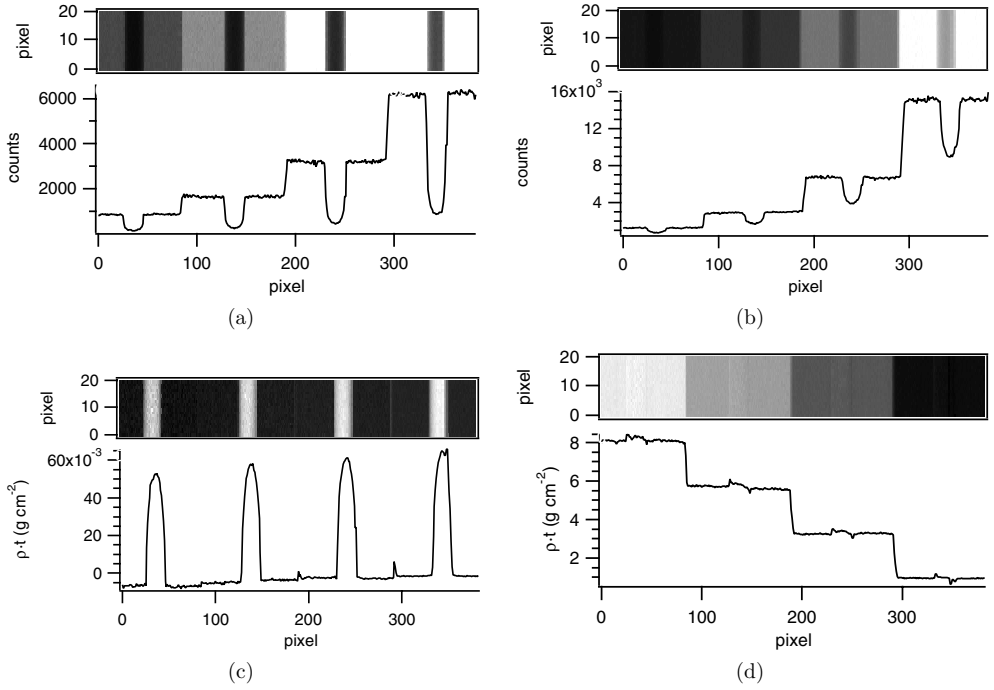

Figure 3. (a) High-energy image, (b) low-energy image, (c) *iodine* image and (d) *water* image of the phantom with vessel diameter equal to 2 mm filled with an iodine concentration of 370 mg ml^{-1}.

Table 2. Signal and SNR of 2 mm diameter vessels calculated at various iodine concentrations.

	Vessel 1		Vessel 2		Vessel 3		Vessel 4	
Concentration (mg ml^{-1})	Signal (g cm^{-2})	SNR	Signal (g cm^{-2})	SNR	Signal (g cm^{-2})	SNR	Signal (g cm^{-2})	SNR
370.0	6.0×10^{-2}	180	6.2×10^{-2}	65	6.4×10^{-2}	261	6.7×10^{-2}	951
185.0	3.0×10^{-2}	73	3.1×10^{-2}	37	3.1×10^{-2}	95	3.2×10^{-2}	350
92.5	1.6×10^{-2}	28	1.7×10^{-2}	21	1.7×10^{-2}	54	1.8×10^{-2}	201
46.3	0.8×10^{-2}	15	0.4×10^{-2}	12	0.7×10^{-2}	32	0.6×10^{-2}	70
23.1	0.5×10^{-2}	13	0.5×10^{-2}	6	0.4×10^{-2}	17	0.4×10^{-2}	35
11.6	–	–	0.2×10^{-2}	5	0.3×10^{-2}	7	0.3×10^{-2}	22

behaviour compared to the other chips. For this reason the signal of the second vessel, that is in correspondence with displacement from the second and third read-out chips, has been affected.

In all the iodine images the background decreases from right to left. This trend is mainly due to a beam hardening effect which causes a negative background signal after image processing. Since the diffracted beams are not monoenergetic, the mean energies E_+ and E_- slightly change when crossing the phantom. This energy shift depends on step thickness and composition so, to correctly address the residual background in the subtraction image, a phantom which simulates bone and tissue density variation should be used.

For each image we have measured the signal and the SNR values for the four cavities and the results are reported in tables 2 and 3.

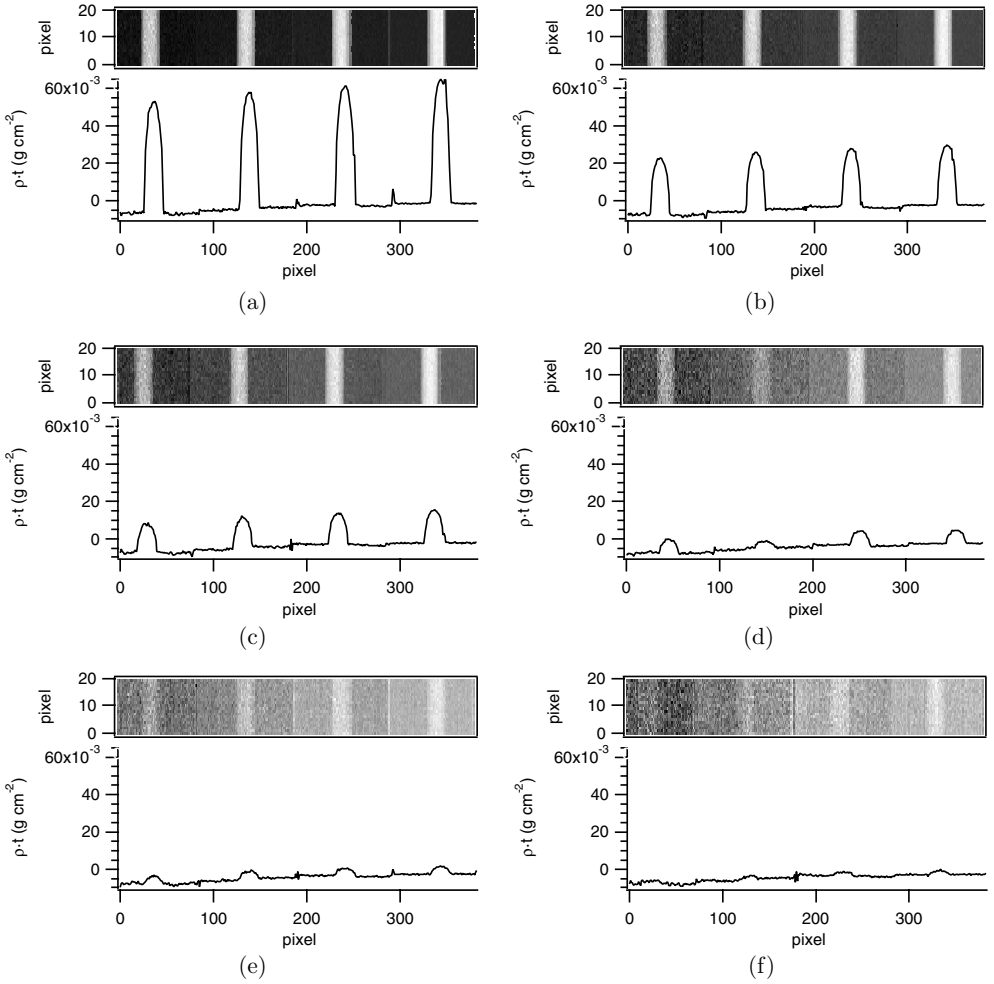

Figure 4. *Iodine* images and profiles of the test object with vessel diameter equal to 2 mm filled with iodine concentration (a) 370 mg ml^{-1}, (b) 185 mg ml^{-1}, (c) 92.5 mg ml^{-1}, (d) 46.3 mg ml^{-1}, (e) 23.1 mg ml^{-1} and (f) 11.6 mg ml^{-1}. The step thickness decreases from left to right and the profiles are the average of counts calculated for the 20 scans.

Table 3. Signal and SNR of 1 mm diameter vessels calculated at various iodine concentrations.

	Vessel 1		Vessel 2		Vessel 3		Vessel 4	
Concentration (mg ml^{-1})	Signal (g cm^{-2})	SNR	Signal (g cm^{-2})	SNR	Signal (g cm^{-2})	SNR	Signal (g cm^{-2})	SNR
370.0	3.2×10^{-2}	80	3.4×10^{-2}	46	3.2×10^{-2}	94	3.1×10^{-2}	360
185.0	1.6×10^{-2}	45	1.2×10^{-2}	17	1.3×10^{-2}	52	1.5×10^{-2}	140
92.5	0.8×10^{-2}	23	0.8×10^{-2}	13	0.8×10^{-2}	32	0.9×10^{-2}	90
46.3	0.5×10^{-2}	10	0.5×10^{-2}	6	0.4×10^{-2}	16	0.4×10^{-2}	40
23.1	0.3×10^{-2}	3	0.4×10^{-2}	4	0.2×10^{-2}	7	0.2×10^{-2}	12
11.6	–		–	–	–	–	0.1×10^{-2}	3

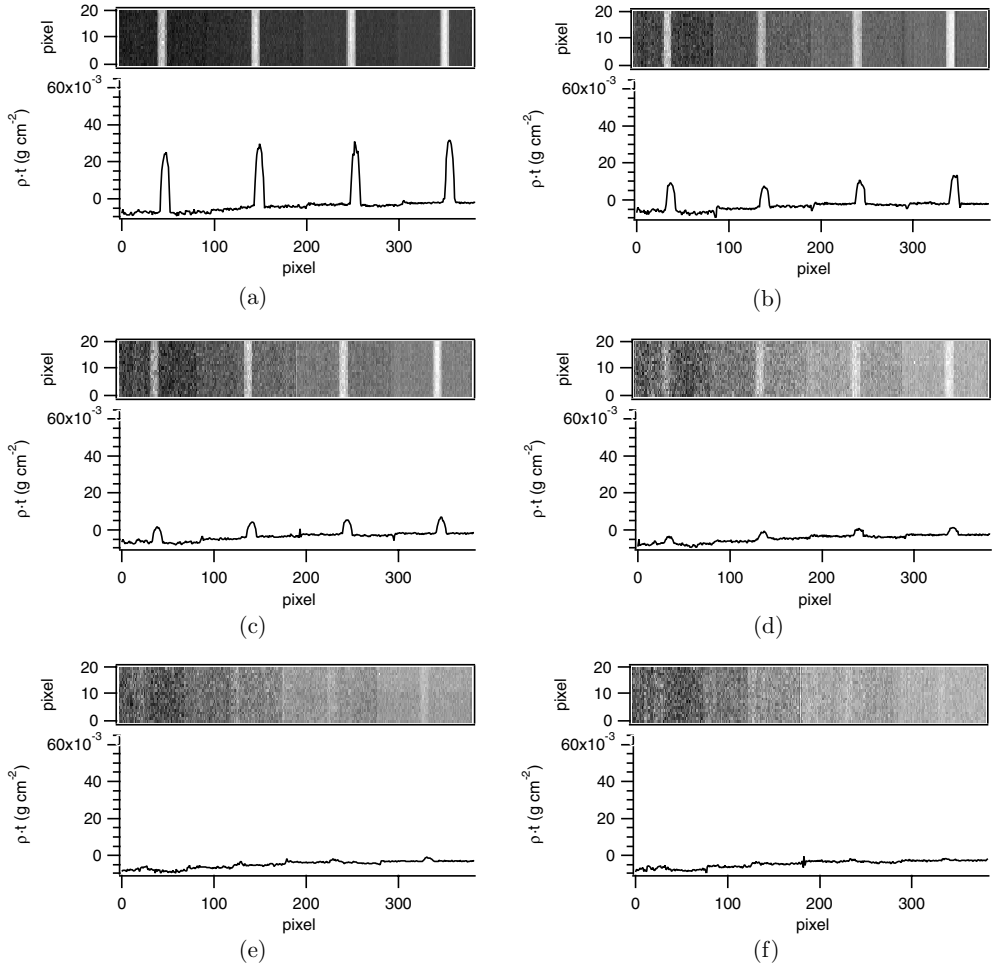

Figure 5. *Iodine* images and profiles of the test object with vessel diameter equal to 1 mm filled with iodine concentration (a) 370 mg ml^{-1}, (b) 185 mg ml^{-1}, (c) 92.5 mg ml^{-1}, (d) 46.3 mg ml^{-1}, (e) 23.1 mg ml^{-1} and (f) 11.6 mg ml^{-1}. The step thickness decreases from left to right and the profiles are the average of counts calculated for the 20 scans.

For each concentration the signal values are almost constant and decrease linearly with the concentrations and the vessel diameter. The plots in figure 7 show the comparison between the measurements for the four cavities and the theoretical expectations obtained by using equation (9). For the highest concentrations the disagreement between the measured and expected contrast value is about 10%. The agreement is better at high dilution. This may be due to the contrast medium approximation. In fact, the contrast medium is based on the iopromide salt in aqueous solution but in the theoretical calculation the contrast medium has been approximated with the iodine and water solution only and the salt composition has been neglected (see equations (9) and (10)).

The SNR values reported in tables 2 and 3 increase from vessel 1 to vessel 4. This trend agrees with the theoretical expectation because the decrease of step thickness leads to a decrease of the σ_{Poisson} (see equation (11)). For the concentration equal to 11.6 mg ml^{-1} (see tables 2 and 3) it was not possible to measure the signal and the SNR because the vessel signal

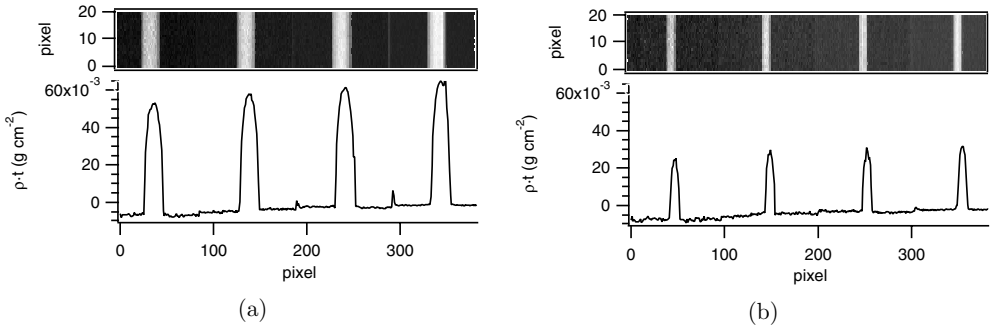

Figure 6. Comparison between the *iodine* images of the test object with vessel diameter equal to (a) 2 mm and (b) 1 mm, filled with an iodine concentration of 370 mg ml^{-1}.

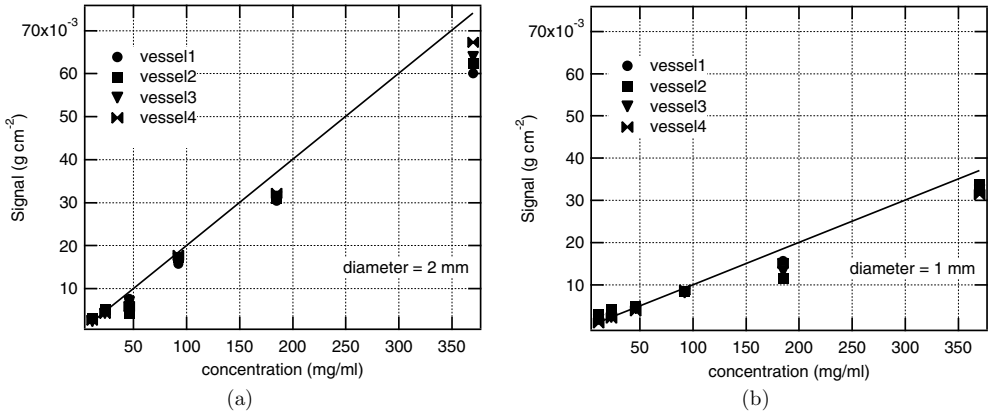

Figure 7. Signal versus concentration for the four vessels with diameter equal to 2 mm (a) and 1 mm (b). The step thicknesses containing the four vessels are: 40 mm of Plexiglas, 6 mm of aluminium (vessel 1); 30 mm of Plexiglas, 4 mm of aluminium (vessel 2); 20 mm of Plexiglas, 2 mm of aluminium (vessel 3); 10 mm of Plexiglas (vessel 4).

and the noise pattern are not separated. The SNR values have been plotted as a function of concentrations for both diameter vessels (see figure 8). The SNR values for the second vessel of the phantom are lower than those for the first cavity for both diameters, in contrast to the theoretical expectations. This disagreement is due to the systematic error introduced by the detector read-out chips board as discussed above. Following the Rose model (Rose 1973) we have assumed the SNR threshold in visual detection equal to 5 (see figure 8). The four cavities with 2 mm diameter have the SNR values above the threshold value for concentrations higher than 23.1 mg ml^{-1}; the threshold concentration of the four cavities with 1 mm diameter is 46.3 mg ml^{-1}.

In figure 9 a comparison between the measured and expected SNR values as a function of concentration is reported. This is only shown in the case of lowest noise, that corresponds to vessel 4 (see equation (11)). The curves are slightly different: the disagreement is mainly due to the electronic noise that has been neglected in the theoretical evaluation.

The possible clinical use of the proposed system depends on the specific examination. For angiography application there are a number of issues that need to be addressed. Since the below- and the above-the-edge beams are adjacent to each other, the two scanned images

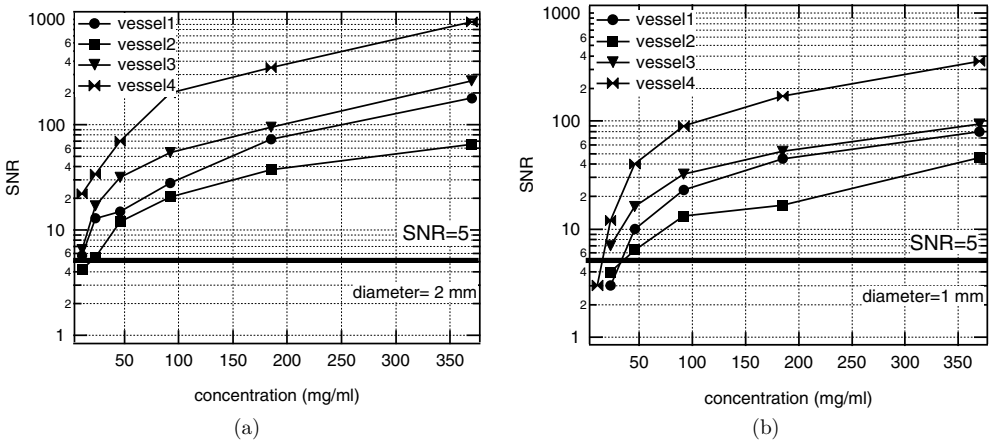

Figure 8. SNR versus concentration for the four vessels with diameter equal to 2 mm (a) and 1 mm (b). The step thicknesses containing the four vessels are: 40 mm of Plexiglas, 6 mm of aluminium (vessel 1); 30 mm of Plexiglas, 4 mm of aluminium (vessel 2); 20 mm of Plexiglas, 2 mm of aluminium (vessel 3); 10 mm of Plexiglas (vessel 4).

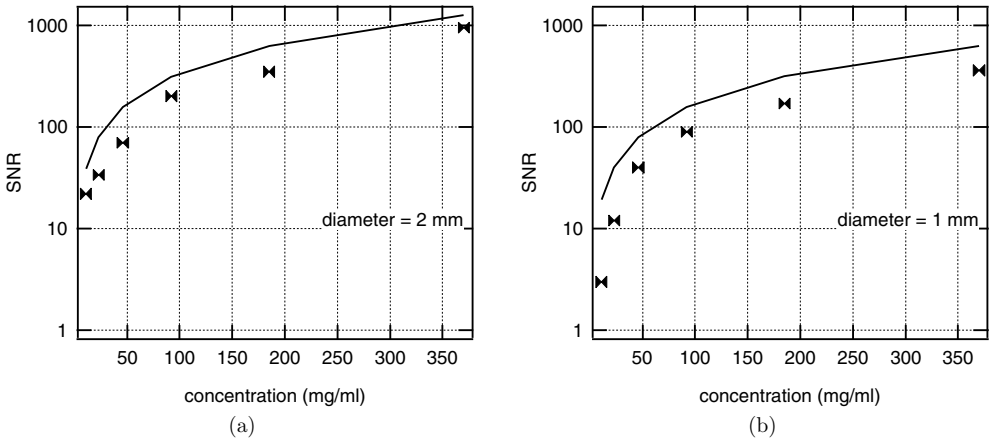

Figure 9. Experimental and theoretical SNR versus concentration for vessel 4 with diameter equal to 2 mm (a) and 1 mm (b).

are not recorded simultaneously. The time elapsed between two exposures may limit the applicability of the method because of the possible body motion. A second issue that needs to be further investigated is the influence of the large separation of the two energies on examination sensitivity. Work is in progress to compare the SNR of the iodine image as a function of the energy separation (Gambaccini *et al* 2003). Furthermore, due to current limitations of the prototype x-ray system, imaging of the test phantom was carried out with object thicknesses less than patient thickness. This means that the system performance is not directly comparable in terms of dose to the subject. As far as mammography is concerned, the photon flux provided by the compact x-ray source may prove to be adequate. Indeed, previous studies showed that, in the mammography energy range, improvements are within the achievable increase of intensity (Gambaccini *et al* 2001). Since at iodine K-edge energies the x-ray beam is more penetrating we only need to optimize the optical system for maximum

reflectivity. However, in contrast-enhanced imaging of the breast, smaller concentrations of iodine are needed than those used here. Again, to investigate the potential of the proposed method in contrast-enhanced mammography, a pre-clinical evaluation has to be undertaken.

5. Conclusions

This study is intended as a first approach to the K-edge digital subtraction technique by using a compact x-ray system. A study concerning the image quality has been carried out as a function of the contrast medium concentration used to fill the vessel inside the phantom. The agreement between calculation and experiment is very good, which suggests that calculations can be used for further optimization of the image system and image acquisition. The obtained results are the starting point for further investigations concerning improvements of compact source and delivered dose with the aim of testing the system for contrast-enhanced techniques in the field of medical imaging.

References

Baldazzi G *et al* 2002 Imaging characterization of an experimental apparatus for dual-energy angiography *IEEE NSS MIC Conf. Record (Norfolk, VA, 10–16 Nov. 2002)*

Baldazzi G *et al* 2003a Result about imaging with silicon strips for angiography and mammography *Proc. VII Mexican Symp. on Medical Physics (Mexico City 24–26 March 2003)*

Baldazzi G *et al* 2003b X-ray imaging with a silicon microstrip detector coupled to the RX64 ASIC *Nucl. Instrum. Methods* A **509** 315–20

Baldazzi G *et al* 2003c A silicon strip detector coupled to the RX64 ASIC for X-ray diagnostic imaging *Nucl. Instrum. Methods* A **514** 206–14

Dabin Y *et al* 2001 A patient position system for the ESRF medical imaging facility *Nucl. Instrum. Methods* A **467–468** 1342–5

Del Guerra A *et al* 2003 A dedicated system for breast cancer study with combined SPECT-CT modalities *Nucl. Instrum. Methods* A **497** 129–34

Dill T, Dix W-R, Hamm C W, Jung M, Kupper W, Lohmann M, Reime B and Ventura R 1998 Intravenous coronary angiography with synchrotron radiation *Eur. J. Phys.* **19** 499–511

Dix W-R 1995 Intravenous coronary angiography with synchrotron radiation *Prog. Biophys. Mol. Biol.* **63** 159–91

Dix W-R, Kupper W, Dill T, Hamm C W, Job H, Lohmann M, Reime B and Ventura R 2003 Comparison of intravenous coronary angiography using synchrotron radiation with selective coronary angiography *J. Synchrotron Rad.* **10** 219–27

Elleaume H *et al* 1999 Instrumentation of the ESRF medical imaging facility *Nucl. Instrum. Methods* A **428** 513–27

Elleaume H *et al* 2000 First human transvenous angiography at the European Synchrotron Radiation Facility *Phys. Med. Biol.* **45** L39–43

Gambaccini M, Taibi A, Del Guerra A, Frontera F and Marziani M 1995 Narrow energy bands x-rays via mosaic crystal for mammography application *Nucl. Instrum. Methods* A **365** 248–54

Gambaccini M, Taibi A, Del Guerra A and Frontera F 1996 Small-field imaging properties of narrow energy band x-ray beams for mammography *IEEE Trans. Nucl. Sci.* **43** 2049–52

Gambaccini M, Tuffanelli A, Taibi A and Del Guerra A 2001 Spatial resolution measurements in quasi-monochromatic X-rays with mosaic crystals for mammography application *Med. Phys.* **28** 412–8

Gambaccini M, Tuffanelli A, Taibi A, Fantini A and Del Guerra A 1999 Bragg diffraction-based quasi-monochromatic source for mammography using mosaic crystals *Proc. SPIE* **3770** 174–84

Gambaccini M *et al* 2003 Signal-to-noise ratio evaluation in transvenous coronary angiography, Experiment MD-41, European Synchrotron Radiation Facility (unpublished)

Grybos P and Dabrowski W 2001 Development of fully integrated readout for high count rate position sensitive measurements of X-rays using silicon strip detectors *IEEE Trans. Nucl. Sci.* **48** 466–72

Lehmann L A, Macovski A, Brody W R, Pelc N J, Riederer S J and Hall A L 1981 Generalized image combination in dual KVP digital radiography *Med. Phys.* **8** 659–67

Lewin J M, Isaacs P K, Vance V and Larke F J 2003 Dual-energy contrast-enhanced digital subtraction mammography: feasibility *Radiology* **229** 261–8

Rato Mendes P *et al* 2003 Silicon strip detectors for two-dimensional soft x-ray imaging at normal incidence *Nucl. Instrum. Methods* A **509** 333–9

Rose A 1973 *Vision: Human and Electronic* (New York: Plenum)

Skarpathiotakis M, Yaffe M J, Bloomquist A K, Rico D, Muller S, Rick A and Jeunehomme F 2002 Development of contrast digital mammography *Med. Phys.* **29** 2419–26

Tuffanelli A, Fabbri S, Taibi A, Gambaccini M and Sarnelli A 2002a Evaluation of a dichromatic x-ray source for dual-energy imaging in mammography *Nucl. Instrum. Methods* A **489** 71–92

Tuffanelli A, Sanchez Del Rio M, Pareschi G, Gambaccini M, Taibi A, Fantini A and Ohler M 1999 Comparative characterization of highly oriented pyrolytic graphite by means of diffraction topography *Proc. SPIE* **3773** 192–8

Tuffanelli A, Taibi A, Baldazzi G, Bollini D, Gombia M, Ramello L and Gambaccini M 2002b Novel x-ray source for dual-energy subtraction angiography *Proc. SPIE* **4682** 311–9

Wagner R F 1977 Toward a unified view of radiological imaging system. Part II. Noisy images *Med. Phis.* **4** 279–96

Zhong Z, Chapman D, Menk R, Richardson J, Theophanis S and Thomlinson W 1997 Monochromatic energy-subtraction radiography using a rotating anode source and a bent Laue monochromator *Phys. Med. Biol.* **42** 1751–62